GRAS1 non-coding RNA protects against DNA damage and cell death by binding NKAP

Tong Su, Lingbo Kong, Darin Cheung, Jonathan Zhu, Vita Chou, Nichelle Camden, Calvin Huang, and Colleen A. McHugh[†]

Department of Chemistry and Biochemistry, University of California San Diego, La Jolla, CA 92093

[†]To whom correspondence should be addressed: c1mchugh@ucsd.edu

Colleen A. McHugh, Ph.D.
Department of Chemistry and Biochemistry
University of California San Diego
Urey Hall Room 6213
9500 Gilman Drive MC 0314
La Jolla, CA 92093

ABSTRACT

Non-coding RNA (ncRNA) gene products are involved in diverse biological processes, but the biological mechanisms by which ncRNAs may regulate cell survival remain poorly understood. We found that the Growth Regulator Antisense (GRAS1) RNA transcript is a positive regulator of growth. Decreased levels of GRAS1 long non-coding RNA (lncRNA) caused DNA damage, cell death, and upregulated expression of genes associated with p53 signaling pathways. Extensive DNA damage occurred after GRAS1 knockdown, with multiple double strand breaks occurring in each cell. The number of cells arrested with low DNA content in sub-G1 phase increased significantly after GRAS1 knockdown. We used RNA antisense purification and mass spectrometry (RAP-MS) to identify the NF-κB activating protein (NKAP) as a direct protein interaction partner of GRAS1 lncRNA. NKAP protein levels decreased after GRAS1 knockdown, while mRNA levels were not affected. The decrease in NKAP protein after GRAS1 knockdown was blocked by proteasome inhibition. GRAS1 knockdown led to lipid peroxidation and overexpression of NKAP prevented the cell death effects of GRAS1 knockdown. NKAP overexpression protected against DNA damage in GRAS1 knockdown cells. We concluded that GRAS1 lncRNA binds and stabilizes NKAP to promote cell survival and protect against DNA damage and cell death.

INTRODUCTION

Non-coding RNAs (ncRNAs) are a large class of biomolecules with the potential to regulate cancer signaling and cell growth processes. Over 20,000 genes in the human genome produce ncRNA transcripts, and dysregulation of ncRNA expression has been associated with cancer growth and tumorigenesis (Kazemzadeh et al. 2015, Wang and Chang, 2011). Direct interactions between non-coding RNA and proteins can regulate critical biological processes in humans. For example, the XIST long non-coding RNA coordinates the spatial and temporal localization of the SHARP/NCOR2/HDAC3 complex to initiate epigenetic silencing of the X chromosome during female development (McHugh et al. 2015). Understanding the mechanisms by which ncRNA transcripts function in cell growth and development can provide new insights into the underlying biology of cancer initiation and progression and lead to the development of more effective and personalized therapies. In this study, we examined the ability of the Growth Regulator Antisense RNA 1 (GRAS1) to affect cell growth in a model lung cancer cell line.

Lung cancer remains a leading cause of mortality worldwide. Only 19% of patients survive for five years or more after diagnosis and approximately 50% of patients with non-small cell lung cancer (NSCLC) experience tumor recurrence (Uramoto and Tanaka, 2014). Genetic variation in individuals may affect the risk of developing non-small cell lung cancer and contribute to drug resistance to small molecule or immunotherapy treatments. A more complete understanding of the molecular interactions and gene products contributing to cancer cell growth and survival would enable the development of new therapeutics and early detection assays for lung cancer.

GRAS1 is a non-coding RNA produced by a gene locus which was previously identified as a regulator of cancer cell growth in a CRISPR/Cas9 screen (Liu et al. 2017). We examined the expression of GRAS1 in RNA-seq data from multiple cancer lines and found that a shorter isoform was the predominant RNA expressed in many cell types. Knockdown of GRAS1 significantly decreased cell survival in a non-small cell lung cancer cell line and led to extensive DNA damage and cell death. Overexpression of GRAS1 conversely increased cell growth. We evaluated the transcriptomic changes induced by GRAS1 knockdown and found that downregulation of GRAS1 lncRNA expression induced activation of the p53 pathway and disrupted cell cycle progression. We found that GRAS1 directly interacts with NKAP protein in cells by using a highly denaturing RNA antisense purification technique coupled with mass spectrometry to purify endogenous GRAS1-protein complexes. When GRAS1 RNA expression was downregulated, protein levels of NKAP also decreased significantly, leading to an increase in cell death and lipid peroxidation. Finally, overexpression of NKAP could protect against the growth effects of GRAS1 knockdown in A549 lung cancer cells. Post-translational regulation of protein stability by RNA binding is an understudied mechanism of cellular control. We report that GRAS1 RNA contributes to the maintenance of cell survival through a direct interaction with the NKAP protein.

RESULTS

GRAS1 non-coding RNA knockdown and overexpression affect A549 cell growth

The GRAS1 non-coding RNA gene is located at Chromosome 5q22.1 and comprises a portion of the NCBI Refseq annotated transcript NR_015370.2, also called EPB41L1A-AS1. A

shorter isoform of this gene locus, referred to here as GRAS1 (Transcript coordinates, hg38 Chr5: 112,160,901-112,162,501), is predominantly expressed in A549 and many other cell types for which RNA sequencing data is available from ENCODE (Figure 1A). The subcellular localization of GRAS1 lncRNA was evaluated in A549 cells, and GRAS1 was detected in both nuclear and cytoplasmic fractions by qRT-PCR. Control GAPDH mRNA and U1 snRNA were observed predominantly in the cytoplasmic and nuclear fractions, respectively, concordant with their cellular functions (Fig. 1B). Based on this dual localization, GRAS1 may function in both the nucleus and cytoplasm of A549 cells.

We evaluated whether GRAS1 affects cell growth and survival of non-small cell lung cancer cells. Overexpression or knockdown of the GRAS1 transcript was performed in A549 cells. For knockdown of GRAS1, we designed two independent GapmeRs targeting different regions of the RNA, to reduce the possibility that any observed knockdown phenotypes might be due to off-target effects (Fig. 1C). The GapmeR knockdown approach was chosen instead of genetic deletion to avoid potential disruption of DNA regulatory elements at the gene locus. We consistently and reproducibly achieved knockdown of around 60% of the GRAS1 transcript in A549 cells after treatment with either of the GRAS1-targeting GapmeRs, compared to a non-targeting control GapmeR. We found that knockdown of GRAS1 dramatically decreased the cell survival of A549 non-small cell lung cancer cells based on the MTT assay for mitochondrial function (Fig. 1D). A colony formation assay validated the result of the MTT assay and revealed that GRAS1 knockdown significantly impaired cell survival and colony growth (Fig. 1E, Supplementary Fig. 1D).

Next, we evaluated the effects of overexpression of GRAS1. The GRAS1 non-coding RNA transcript sequence was amplified from human cDNA and cloned into pcDNA3.2 under

control of the cytomegalovirus (CMV) promoter. A549 cells transfected with pcDNA-GRAS1 plasmid efficiently overexpressed GRAS1 ncRNA compared to A549 cells transfected with the pcDNA control vector (Fig. 1F). We found that overexpression of GRAS1 significantly increased the survival of A549 cells in the MTT assay (Fig. 1G). To further validate this result, a colony formation assay was used to evaluate A549 cell growth. Overexpression of GRAS1 in A549 cells increased colony formation compared to the vector-only control (Fig. 1H). In conclusion, GRAS1 non-coding RNA is critical for A549 cell survival, and depletion of the GRAS1 lncRNA transcript leads to cell death.

GRAS1 knockdown cells increase transcription of DNA damage response and cell cycle related genes

Since knockdown of GRAS1 led to a dramatic decrease in cell survival, we used high-throughput RNA sequencing to evaluate alterations in gene expression after GRAS1 knockdown in A549 cells and determine which cellular pathways were affected by GRAS1 function. Transcriptome-wide changes in RNA levels in GRAS1 knockdown cells were measured after 48 hours of GapmeR treatment, with 20 to 40 million reads per sample obtained by Illumina sequencing. Principal Component Analysis (PCA) showed clustering of independent biological replicate samples for each treatment and indicated a clear separation between knockdown and control samples across the two treatment sets (Fig. 2A). Knockdown efficiency of GRAS1 in the treated samples was confirmed using normalized read counts from the aligned RNA sequencing data. We also confirmed that the neighboring antisense gene EPB41L4A and a snoRNA contained within the GRAS1 transcript did not show significant changes in RNA expression levels after GRAS1 GapmeR treatment (Figure S1).

Knockdown of GRAS1 lncRNA led to alterations in expression levels of many genes. In the differentially expressed gene set, 41.4% of genes were upregulated in expression and 58.6% of genes were downregulated in expression (Fig. 2B). We identified a total of 12,062 genes that were more than 2-fold differentially expressed with p value ≤ 0.05 (Fig. 2C). For gene ontology analysis of GRAS1-affected transcripts, we used the top 1,000 differentially expressed genes based on p value from expression level changes in three biological RNA-seq replicates of GRAS1 knockdown versus control GapmeR treatment. Gene ontology (GO) enrichment analysis of the differentially expressed genes identified alterations in pathways related to cell survival (Fig. 2D). Heatmaps of the top 20 upregulated genes in GRAS1 knockdown cells, sorted based on the p value, from the TP53 protein (p53) signaling pathway, DNA damage response, and cell cycle control are shown in Figure 2E. Downregulated transcripts were associated with multiple cellular pathways including spindle formation and chromosome condensation. We found that GRAS1 knockdown leads to differential expression of many mRNA transcript levels, including cell survival related pathways such as p53 signaling, DNA damage response, and cell cycle regulation.

GRAS1 knockdown causes accumulation of multiple DNA damage foci and cell death

Based on the upregulation of p53 target genes by RNA-seq, we next investigated whether DNA damage occurred in GRAS1 knockdown cells. We also evaluated whether GRAS1 knockdown affects the p53 signaling pathway, since p53 is a key regulator of cell viability and cell cycle progression in response to DNA damage and other types of cell stress (Kastan et al. 1995). Knockdown of GRAS1 significantly increased p53 protein levels in cells (Fig. 3A). Consistent with this result, we found that knockdown of GRAS1 also increased the mRNA expression of p53 gene targets including p21, PML, PLK3, and Gadd45a (Fig. 3B). These

findings were further validated by quantifying normalized read counts from the RNA-seq data (Fig. S2). TP53 mRNA levels were not as strongly affected as p53 protein levels in GRAS1 knockdown cells (Fig. S2). The overexpression of GRAS1 lncRNA had no effect on the protein level of p53 or the expression of p53 gene targets (Fig. S2). We concluded that the downregulation of GRAS1 RNA transcript activates p53 signaling in A549 cells.

The p53 signaling pathway can be activated by DNA damage (Lakin and Jackson, 1999). Based on the observation of a strong upregulation of DNA damage response genes by RNA-seq, we investigated whether knockdown of GRAS1 increases DNA damage in A549 cells. Histone H2AX phosphorylation was evaluated by Western blot in GRAS1 knockdown cells as an indicator of DNA damage. The histone variant H2AX is rapidly phosphorylated at Serine 139 (γH2AX) in an early cellular response to DNA double strand breaks (Mah et al. 2010). Knockdown of GRAS1 significantly increased the overall levels of γH2AX modified protein (Fig. 3A). No significant alteration in γH2AX level was observed when GRAS1 was overexpressed in A549 cells (Fig. S2). We then performed an immunofluorescence assay to enumerate γH2AX foci in individual cells using confocal microscopy. The γH2AX foci visualized in cell nuclei by this assay directly correlate with the locations of double-strand breaks in DNA (Mah et al. 2010). Consistent with the results of γH2AX immunoblotting, we found that knockdown of GRAS1 significantly increased the number of γH2AX foci, with many cells containing dozens of foci (Fig. 3C). These results indicate that downregulation of GRAS1 leads to a significant increase in DNA damage in A549 cells. Chromosome condensation and DNA fragmentation is a typical characteristic of programmed cell death after DNA damage is incurred (Toné et al., 2007). We also observed that knockdown of GRAS1 severely affected nuclear morphology in A549 cells after 48 hours of GapmeR treatment (Fig. 3D). These data indicate

that the downregulation of GRAS1 induces extensive DNA damage through double-strand breaks in A549 cells and affects the nuclear morphology.

GRAS1 affects cell cycle distribution in A549 cells

Regulation of the cell cycle plays a critical role in maintaining cell viability by ensuring that the cell replicates and divides correctly with appropriate DNA content and integrity through each phase of the cycle. To assess the role of GRAS1 in cell cycle regulation, we performed propidium iodide (PI) staining and flow cytometry analysis on GRAS1 knockdown or overexpression cells. Downregulation of GRAS1 led to a significant increase in the number of cells with low DNA content (sub-G1 phase) compared to control cells, indicating that a larger proportion of cells in the population were undergoing apoptosis or contained fragmented chromosomes after GRAS1 knockdown (Fig. 3E). Loss of GRAS1 also decreased the proportion of cells in G1 phase. In contrast, overexpression of GRAS1 led to a decrease in cell number in the sub-G1 phase, and an increase in the number of cells in G1 phase (Fig. 3F). These data indicate that depletion of GRAS1 RNA affects the cell cycle distribution of A549 cells in culture.

GRAS1 non-coding RNA binds and stabilizes NF-κB activating protein (NKAP)

To investigate the biological mechanism by which GRAS1 regulates cell growth, we identified direct protein interaction partners of the endogenous GRAS1 RNA transcript in A549 cells using RNA antisense purification with mass spectrometry (RAP-MS). First, we validated the capture and recovery of GRAS1 RNA by sequence-specific biotinylated antisense oligonucleotide probes on streptavidin beads (Fig. 4A). We then used RAP-MS to purify endogenous RNA-protein complexes from UV_{254nm}-crosslinked cells and identify direct and specific protein binding

partners of the GRAS1 lncRNA. Identified GRAS1 interacting proteins were compared to proteins found in the U1 snRNA positive control and the luciferase mRNA negative control (Fig. 4B). We identified 63 proteins in the luciferase control capture, 256 proteins in the U1 control capture, and 192 proteins in the GRAS1 specific capture sample. After removing any proteins found in the luciferase negative control capture, there were still 138 identified proteins remaining in the GRAS1 capture sample and 208 identified proteins in the U1 capture sample. To filter out common RNA-binding proteins and splicing factors from the GRAS1 interactome list, we then removed any proteins which were bound by both U1 snRNA and GRAS1 RNA. A total of 21 proteins were found to be direct and specific interacting factors of GRAS1 lncRNA, with at least two unique peptides identified by mass spectrometry (Fig. 4C). These are direct RNA-protein interaction partners, because the UV crosslinking approach used in RAP-MS experiments can only covalently crosslink "zero-distance" binding interactions between nucleobases and aromatic amino acids. The use of a highly denaturing wash buffer containing 4 M urea and 500 mM lithium chloride eliminates indirect protein interactions as well as non-specific binding proteins which depend upon electrostatic interactions occurring in solution after cell lysis (McHugh et al. 2015, McHugh, Russell and Guttman 2015).

NKAP and C11ORF57/NKAPD1 were identified in our screen as the top interaction partners of GRAS1 lncRNA. NKAP was previously characterized as an RNA-binding protein (Burgute and Noegel, 2014) and protects glioblastoma cells against ferroptosis and cell death (Sun et al. 2022). In HeLa cells, NKAP is required for centrosome assembly and sister chromatid separation (Li et al. 2016). The function of C11ORF57/NKAPD1 remains uncharacterized. Therefore, we focused the remainder of our studies in this work on the NKAP protein, to investigate whether the direct interaction between GRAS1 and NKAP is related to the effects of

cell survival in A549 caused by GRAS1 lncRNA knockdown. To validate the interaction between GRAS1 and NKAP with an orthogonal approach, we performed an RNA immunoprecipitation (RIP) experiment in non-crosslinked A549 cell lysates, by capturing NKAP and testing for GRAS1 by qRT-PCR. We observed more than a 50-fold increase in GRAS1 RNA capture in NKAP-IP elution compared to control IgG elution (Fig. 4D).

Since GRAS1 interacts directly with NKAP in A549 cells, we investigated the effect of GRAS1 knockdown on NKAP mRNA and protein levels. Notably, knockdown of GRAS1 did not affect NKAP mRNA levels (Fig. 4E) but instead caused a significant decrease in the protein level of NKAP (Fig. 4F). Therefore, we concluded that GRAS1 lncRNA may have a post-translational effect to regulate either NKAP stability or degradation. Treatment of GRAS1 knockdown cells with the proteasome inhibitor MG132 prevented the decrease in protein level of NKAP (Fig. 4F). The combined data from RAP-MS and RIP indicated that GRAS1 lncRNA binds directly to NKAP in A549 cells, and that GRAS1 RNA protects NKAP from proteasomal degradation.

NKAP overexpression reverses the lipid peroxidation induced by GRAS1 knockdown

We next examined the contribution of the GRAS1-NKAP interaction to cell survival. GRAS1 knockdown cells showed extensive DNA damage responses and p53 activation, which could arise from multiple pathways including oxidative stress and ferroptotic cell death. NKAP was previously shown to protect glioblastoma cells from ferroptosis (Sun et al, 2022). A key marker for ferroptosis is lipid peroxidation in cell membranes, which can be detected using a BODIPY-C11 reporter in a flow cytometry assay (Martinez et al, 2020). We found that GRAS1 knockdown significantly increased lipid peroxidation in A549 cells (Fig. 5A). Addition of the ferroptosis inhibitor compound ferrostatin (Fig. 5B) or the antioxidant α-tocopherol (Fig. 5C)

reversed the effect of lipid peroxidation caused by GRAS1 knockdown. We also observed a decrease in lipid peroxidation in cells with GRAS1 lncRNA overexpression alone, without any knockdown GapmeR or other treatment (Fig. 5D). Next, we overexpressed NKAP in A549 cells (Fig. 5E) and observed that NKAP expression increased cell viability compared to an eGFP control vector (Fig. 5F). Using flow cytometry, we found that overexpression of NKAP reduced the level of lipid peroxidation in GRAS1 knockdown cells (Fig. 5G). NKAP overexpression alone also resulted in reduced levels of lipid peroxidation compared to control cells (Fig. S3). Perturbation of GRAS1 and NKAP had significant effects on lipid peroxidation. We concluded that GRAS1 induces lipid peroxidation to cause cell death in A549, and NKAP overexpression can rescue the loss of GRAS1 lncRNA and the cell death phenotype.

Overexpression of NKAP prevents DNA damage in GRAS1 knockdown cells

To determine whether ferroptosis is a main contributor to DNA damage after GRAS1 knockdown, we performed rescue experiments with ferrostatin treatment or NKAP overexpression in GRAS1 knockdown cells. Ferrostatin treatment could not rescue the DNA damage phenotype of GRAS1 knockdown (Fig. 6A). However, overexpression of NKAP slightly decreased the levels of γH2AX in GRAS1 knockdown cells treated with GapmeR1 and significantly decreased γH2AX levels in GRAS1 knockdown cells treated with GapmeR2 (Fig. 6B). Using an Annexin V and propidium iodide staining flow cytometry assay for apoptotic cells, we found that knockdown of GRAS1 significantly decreased the live cell population in GRAS1 knockdown cells compared to cells treated with control GapmeR (Fig. 6C). The apoptotic cell population marked by annexin V staining increased in GRAS1 knockdown cells. Overexpression of GRAS1 alone had the opposite effect and resulted in an increase in cell survival, similar to the phenotype observed in the MTT and colony formation assays (Fig. S4).

Finally, we tested if overexpression of NKAP could reverse the effect of GRAS1 downregulation. We observed that expression of NKAP protected cells from cell death and abrogated the effect of GRAS1 knockdown in the Annexin V and PI staining assay (Fig. 6D). In summary, we found that NKAP protects A549 cells against the cellular effects of GRAS1 downregulation.

DISCUSSION

Non-coding RNAs may act as regulators of cell survival and cell death pathways. We identified a role for the GRAS1 long non-coding RNA in promoting cell survival in the non-small cell lung cancer cell line A549. Further, we identified NKAP as a direct interaction partner of GRAS1 lncRNA and found that GRAS1 prevents NKAP degradation to protect against DNA damage, cell cycle arrest, and cell death.

The GRAS1 non-coding RNA locus has been previously implicated in cell growth control, including in gastric cancer (Delshad et al. 2019), lung cancer (Wang et al. 2020), colorectal cancer (Bin et al. 2021), cervical cancer (Liao et al. 2019) and placental villus (Zhu et al. 2019). GRAS1 may also affect proliferation and cell cycle phase distribution in bone marrow-derived mesenchymal stem cells (Cui et al. 2020). Transcriptomics and gene ontology analysis of differentially expressed genes in GRAS1 knockdown versus control cells revealed the upregulation of multiple pathways related to cell survival, including p53 activation, DNA damage response, and cell cycle control. We used these transcriptomic data as a guide to further investigate the phenotypic effects of GRAS1 knockdown in non-small cell lung cancer cells.

Knockdown of GRAS1 activated p53 and increased the mRNA level of downstream p53 target genes in A549 cells. No significant changes were observed on the p53 level or expression

of the p53 downstream target genes when GRAS1 was overexpressed. Mammalian cells generally maintain a low level of p53, due to continual degradation and rapid turnover (Lakin and Jackson 1999). Cellular p53 accumulation can be caused by multiple stressors, including DNA damage, metabolic alterations, hypoxia, abnormal oncogenic expression, and cytokine activations (Lakin and Jackson 1999). GRAS1 knockdown significantly increased DNA damage, as measured by quantification of the DNA damage marker γH2AX. In many of the GRAS1 knockdown cells, more than 50 double-strand breaks were observed within a single cell. It is unclear how extensive DNA damage can be induced by GRAS1 knockdown after only 24 hours of treatment.

We found that GRAS1 depletion affects the cell cycle distribution in A549 cells. Significant changes in the sub-G1 cell population indicated that GRAS1 knockdown results in cells with low DNA content, suggesting that an increased number of cells in the population are undergoing programmed cell death processes (Shu et al. 1997).

We used RAP-MS, an effective tool for identifying specific and direct protein interacting partners with endogenous RNA molecules, to identify GRAS1 interaction partners. We found 21 proteins that directly interact with GRAS1 using the RAP-MS method and focused our subsequent complementation studies on NKAP. The interaction between NKAP and GRAS1 was validated by immunoprecipitation and quantitative RT-PCR (qRT-PCR). NKAP is a multifunctional protein essential for growth and development in highly proliferative cells including T cells, spermatozoa, and hematopoietic stem cells (Pajerowski et al. 2009, Shapiro et al. 2019, Okuda et al. 2015). Although NKAP was first identified in yeast (Chen et al. 2003), it has since been characterized as an RNA-binding protein in humans (Burgute et al. 2014) and is associated with gastric cancer (Wei et al. 2019), colon cancer (Shu et al. 2019), glioblastoma

(Sun et al. 2022) and renal cell carcinoma (Ma et al. 2020). Dysregulation of NKAP causes chromosome segregation defects and genome instability (Li et al. 2016), and NKAP can act as a novel ferroptosis suppressor (Sun et al. 2022). The regulation of NKAP stability by RNA binding has not been previously evaluated. Surprisingly, we found that the knockdown of GRAS1 lncRNA reduced the level of NKAP protein, while the level of NKAP mRNA remained unaffected. Inhibition of proteasomal degradation prevented NKAP degradation upon GRAS1 knockdown. Therefore, we concluded that GRAS1 affects NKAP though a post-translational regulation mechanism affecting stability or degradation of NKAP.

Next, we investigated the cause of cell death in GRAS1 knockdown cells. We found that the interaction between GRAS1 and NKAP protects A549 cells from lipid peroxidation and cell death. Ferroptosis is an iron-dependent mechanism of programmed cell death (Dixon and Stockwell. 2019) and can be regulated by multiple signaling cascades including the p53 pathway (Xu et al. 2019). Indicators of ferroptosis are increased lipid peroxidation and mitochondrial defects (Li et al. 2020). During ferroptosis, an imbalance of intracellular iron leads to accumulation of reactive oxygen species (ROS) and lipid damage, ultimately leading to loss of membrane permeability and cell death (Xu et al. 2019, Chen et al. 2021). Treatment with ferroptosis inhibitors, including ferrostatin and α-tocopherol, reversed the increased level of ferroptosis caused by GRAS1 lncRNA knockdown. In addition, the decrease in cell survival after GRAS1 knockdown could be rescued by ectopic expression of NKAP, suggesting that NKAP is the key factor linking GRAS1 downregulation to the decrease in cell survival in A549 cells. Although ferroptosis is associated with an increase in cellular reactive oxygen species (Xu et al. 2019), the connection between ferroptosis and DNA damage is still poorly understood. Overexpression of NKAP reversed the increased level of DNA damage after GRAS1

knockdown. However, no significant difference was observed in the protein level of γH2AX in A549 with GRAS1 knockdown after treatment with ferroptosis inhibitors, suggesting the increased level of γH2AX by GRAS1 knockdown is not due to the process of ferroptosis. Therefore, we concluded that the GRAS1-NKAP interaction may have multiple functions in promoting cell growth in A549 non-small cell lung cancer cells.

The cellular functions of many of the non-coding RNAs produced by the human genome are still uncharacterized. We found that the non-coding RNA GRAS1 transcript binds and stabilizes NKAP in a non-small cell lung cancer cell line to prevent NKAP degradation. Loss of GRAS1 lncRNA leads to DNA damage, lipid peroxidation and cell death, which can be rescued by NKAP overexpression. Non-coding RNA transcripts can directly bind proteins to affect biological processes, and RNA-mediated regulation of protein stability is an understudied mechanism of cell growth control. The GRAS1-NKAP functional interaction provides a novel method of cellular protection against DNA damage and cell death.

MATERIALS AND METHODS

Cell lines and culture conditions

Human lung adenocarcinoma A549 cell line (ATCC No. CCL-185), human colorectal carcinoma HCT116 cell line (ATCC No. CCL-247), human breast adenocarcinoma MCF7 cell line (ATCC No. HTB-22), human kidney embryonic HEK293 cell line (ATCC No. CRL-1573), and human chronic myeloid leukemia K562 cell line (ATCC, No. CRL-3344) were purchased from ATCC. A549, MCF7, and HEK293 cells were cultured in Eagle's Minimal Essential Medium (EMEM) (Quality Biological, USA); K562 cells were cultured in Iscove's Modified Dulbecco's Medium (IMDM) (Gibco, Life Technologies, USA); HCT116 were cultured in McCoy's 5A Modified

Medium (Gibco, Life Technologies, USA). All mediums were supplemented with 10% fetal bovine serum (Gibco, Life Technologies, USA) and 1% additional L-Glutamine (Corning, USA). All cells were grown in a cell culture incubator at 37 ˚C with 5% CO_2. Cells were tested monthly for mycoplasma.

Plasmid generation and transfection

Gene inserts were generated by PCR from A549 or K562 complementary DNA (cDNA) using locus-specific primers. Entry vectors of the Gateway cloning system were created with the pENTR/D-TOPO Cloning Kit (2402649, Invitrogen, CA, USA). Once the entry vectors were generated, the gene inserts were transferred to pcDNA3.2 destination vectors using the Gateway LR Clonase Enzyme Mix (11791011, ThermoFisher Scientific, USA). For plasmid transfections, cells were seeded with 2 x 10^5 cells/well in 12-well plates overnight before each treatment. Cells in each well were transfected with 1 μg of plasmid using 3.5 μl of Lipofectamine 2000 (ThermoFisher Scientific, USA) in Opti-MEM I reduced serum medium (31985062, Life Technologies, USA) following the manufacturer's suggested protocol.

Gene knockdown

For the GapmeR knockdown, cells in each well were transfected with 50 μM of each lncRNA-target GapmeR (Qiagen) with Negative Control GapmeR A (30300019-2, Qiagen) using 3.5 μl of Lipofectamine 2000 in Opti-MEM I reduced serum medium following the manufacturer's suggested protocol. Samples were incubated for 24 or 48 hours before collection, as indicated in the text. GapmeR target sequence is shown in Key Resource Table.

Nucleic acid isolation and qRT- PCR

Total RNA from all cell treatments was isolated using QIAshredder and RNeasy Mini kit (Qiagen) then further purified or concentrated as needed with RNA Clean & Concentrator kit

(Zymo Research). For cell fractionation experiments, total RNA from each cell fraction was isolated using Qiagen RNeasy columns. DNA isolations were performed using plasmid Miniprep kit (Qiagen). All isolations were performed according to the manufacturer's protocol. 1.5 µg of purified RNA was used for each reverse transcription reaction with 1 µl of Superscript III Reverse Transcriptase (18080085, Invitrogen, USA). Quantitative real-time PCR (qRT-PCR) was performed using ROX Reference Dye (Invitrogen, USA) and SYBR Green Dye (Life Technologies, USA), with fold expression calculated using the $2^{-\Delta\Delta Ct}$ method. Samples were repeated in biological triplicate. Data were normalized to IgG for immunoprecipitation experiments, normalized to GAPDH or Tubulin control genes for qRT-PCR experiments, and normalized to respective RNA amounts for cellular fractionation products.

Western blotting

Following transfection, cells were harvested with trypsin and washed once with 1x PBS. Cells were then mixed with cell lysate buffer, protein inhibitor cocktail (539134, Millipore Sigma), sodium fluoride, and incubated at 95 °C for 10 min before SDS-PAGE separation. Cell lysates were loaded into a 10-well 10% Bis-Tris SDS-polyacrylamide gel along with PageRuler Plus Protein ladder (26619, ThermoFisher Scientific). Proteins were separated at 130V for 90 min and subsequently transferred to 0.2 micron pore size nitrocellulose membrane. Membranes were blocked with the LI-COR Biosciences Intercept Blocking buffer (VWR International) for one hour at room temperature and incubated with primary antibodies overnight at 4 °C on a rocker. The following primary antibodies were used: p65 (10745-1-AP, Proteintech), p-p65 (3033T, Cell Signaling Technology), STAT5 (25656T, Cell Signaling Technology), p-STAT5 (80115-1-RR Proteintech), NKAP (ab229096, Abcam), GAPDH (60004-1-Ig, Proteintech), p53 (10442-1-AP, Proteintech), Actin (66009-1-Ig, Protechtech) , Histone H3 (4499S, Cell Signaling Technology),

and γH2AX (60566SF, Cell Signaling Technology). All antibodies were diluted in 1x TBST. After incubation, membranes were washed four times for 5 min with 1x TBST buffer (TBS with 0.1% Tween-20). Nitrocellulose membrane was then incubated with goat Anti-mouse (102971-154, VWR International) and goat Anti-rabbit (103011-498, VWR International) IRDye-conjugated secondary antibodies for one hour under dark conditions on a rocker. After four 5-min washes, the membrane was imaged with an Odyssey Fc device (LI-COR Bioscience, USA) and analyzed with Empiria Studio software (LI-COR Bioscience, USA).

Cellular Fractionation

For separation of cytoplasmic and nuclear components, the protocol was performed essentially as previously reported (Gagnon et al., 1999) Briefly, 1 x 10^7 A549 cells were collected by trypsinization and resuspended in 1 mL hypotonic lysis buffer (10 mM Tris-HCl pH 7.5, 10 mM NaCl, 3 mM $MgCl_2$, 0.3% NP-40 supplemented with Complete protease inhibitor cocktail (Roche) and 10% glycerol). After 10 min of incubation on ice and a brief vortex of the sample, 60 μL input control for Western Blot was reserved. The remaining lysate was centrifuged for 8 min, 800 x *g* at 4°C. The supernatant was separated and saved as the cytoplasmic fraction, and 5 M NaCl was added to create a final concentration of 140 mM NaCl in the sample. The remaining pellet was washed four times by resuspending in hypotonic lysis buffer and centrifuged for 2 min at 300 x *g*. The supernatants were saved as individual washes. Total nuclear extract was then prepared by suspending the pellet in 0.5 mL nuclear lysis buffer (20 mM Tris-HCl [pH 7.5], 150 mM KCl, 3 mM $MgCl_2$, 0.3% NP-40 supplemented with 1 complete protease inhibitor cocktail). The input sample was sonicated in a water bath for 15 min while the nuclear fraction and the four washes were sonicated on ice with microtip at 25% duty and 4 output for 60 seconds each on a Branson ultrasonicator. After sonication, all samples except input were centrifuged at 18,000 x *g*

for 10 min at 4°C. Supernatants were transferred to fresh tubes and used for Western Blot and RNA isolation. U1 RNA and Lamin A protein were measured as references for the nuclear fraction and GAPDH mRNA and GAPDH protein were measured as references for the cytoplasmic fraction.

Colony formation assay

For colony formation assays, 2 x 10^5 A549 cells were seeded in a 6-well plate and incubated overnight, followed by GapmeR knockdown targeting GRAS1. After 24 h incubation at 37 ˚C and 5% CO_2, transfected cells were collected using trypsin (Corning, USA) and resuspended in 4 ml EMEM medium. Then, 50 µl of resuspended cell solution was added to 36.5 cm^2 cell dishes with 4 ml EMEM medium and incubated for 10 d. Finally, the medium was discarded and the cells were fixed using 500 µl of fixation buffer (3:1 ratio of methanol to acetic acid). Fixed cells were stained with 0.1% crystal violet (Ricca Chemical, TX, USA).

Immunofluorescence assay and microscopy

1 x 10^5 cells were seeded in a tissue culture dish with glass bottom (20102018, FluoroDish, FL, USA) and incubated overnight before transfection. Transfections were performed as described above. After transfection, cells were washed three times with ice-cold PBS, then fixed with chilled 100% methanol at room temperature for 5 min, and washed three times with PBS for 5 min. Cells were permeabilized by treatment with 0.2% Triton X-100 for 10 min at room temperature, then washed three times with PBS for 5 min. Then, cells were incubated in 1% BSA (bovine serum albumin) in PBST (PBS + 0.1% Tween 20) for 30 min blocking using Normal Goat Serum (ab7481, Abcam) at room temperature. Cells were incubated in primary antibodies for 1 hour at room temperature and washed three times with PBS. Then cells were incubated with Goat Anti-Rabbit IgG H&L Secondary Antibody (ab6717, Abcam) for 1 hour and washed 3

times with PBS. Finally, cells were incubated in either 1 μg/mL DAPI DNA stain (4083S, Cell Signaling Technology) or 0.5 μg/ml Hoechst 33342 Reagent (R37165, ThermoFisher Scientific, USA) for 1 min, rinsed with PBS, and imaged using the Eclipse Ti Inverted Microscope (Nikon, Japan) with Nikon's NIS-Elements imaging software.

Protein immunoprecipitation

For each reaction, 3.5 x 10^7 A549 cells were harvested and resuspended in PBS, then an equal volume of cold polysome lysis buffer was added (20 mM Tris-HCl pH 7.5, 50 mM KCl, 10 mM $MgCl_2$, 1 mM DTT, 1X Complete protease inhibitor cocktail (Roche), 200 units/mL RNase inhibitor murine (New England Biolabs)). Cells were lysed by incubation at 4 °C for 5 min followed by incubation at -80 °C for about two hours before centrifuging for 10 min at 20,000 x *g*. The supernatants were collected and divided so that there were 1 x 10^7 A549 cells per sample and 5 x 10^6 cells were saved as whole cell lysate inputs. 75 μL/sample of Dynabeads Protein G (Thermo Fisher Scientific) were washed twice with NT-2 buffer (50 mM Tris-HCl [pH7.5], 150 mM NaCl, 1 mM $MgCl_2$, 0.05% NP-40) and resuspended in 100 μL/sample of NT-2 buffer, with 3 μg of each antibody per sample: IgG as a negative control (10284-1-AP, Protechtech), TDP-43 as a positive control (10782-2-AP, Proteintech), and NKAP. The beads/antibody mixtures were incubated for 90 min at room temperature, then beads were washed six times with NT-2 buffer before resuspending in NET-2 buffer (50 mM Tris-HCl [pH 7.5], 150 mM NaCl, 1 mM $MgCl_2$, 0.05% NP-40, 20 mM EDTA [pH 8.0], 1 mM DTT, 200 units/mL RNase inhibitor murine). Each antibody had the cell lysate supernatant added so the total volume including the NET-2 buffer would be 1 mL. All three samples were incubated overnight at 4 °C with gentle rotation, followed by six washes with NT-2 buffer, then each sample was split in half for protein and RNA analysis. For RNA samples, the beads were resuspended in NLS elution buffer (20 mM

Tris–HCl [pH 8.0], 10 mM EDTA [pH 8.0], 2% NLS, and 2.5 mM TCEP) for proteinase K digest, then the beads were separated and standard RNA silane cleanup with Dynabeads MyOne Silane (Thermo Fisher Scientific) was performed on the supernatant before reverse transcribing the RNA using SuperScript III to perform qRT-PCR. For protein samples, elution 1 was prepared by using 10 µL of 2X Tris-Glycine SDS sample buffer (Thermo Fisher Scientific) was to resuspend beads containing immunocomplexes and incubated at 50 °C for 10 min, then 9 µL of UltraPure water (Invitrogen) and 1 µL of 0.1 M DTT was added to the elution sample. Elution 2 was collected by resuspending the beads in 10 µL of 2X Tris-Glycine SDS sample buffer and 1 µL of 0.1 M DTT and incubating at room temperature for 5 min before adding 9 µL of UltraPure water to bring the final volume of the sample to 20 µL. All protein samples were heated at 95 °C for 10 min before storing at -80 °C.

MTT cell proliferation assay

Viability and proliferation of A549, HCT116, MCF7, K562 and HEK293 cells were determined by modified microculture tetrazolium (MTT) assay (University at Buffalo, State University of New York, NY, USA), based on the enzymatic reduction of 3-(4,5-dimethylthiazol-2-yl)-2,5-diphenyltetrazolium bromide to form formazan crystals by mitochondria and cellular dehydrogenase enzymes. Before any treatment, 1.5 x 10^4 cells were seeded into each well of 96-well flat-bottomed microplates containing medium overnight. The cells were treated/transfected and incubated in a humidified incubator in 5% CO_2 for 48 hours at 37°C, and then the medium was replaced with the working MTT solution following the manufacturer's instructions. The resulting solution was incubated in 5% CO_2 for another 20 min at 37 °C. Formazan crystals were dissolved in 100 µl of DMSO. The plates were then analyzed on the Synergy HTX Multi-Mode

Microplate Reader (Agilent, USA) at 570 nm. Each sample point was assayed with biological triplicate per assay, and cell line experiments were performed at least three times.

Cell cycle analysis with flow cytometry

Following treatment, A549 cells were harvested with trypsin and washed twice with PBS. Cells were then permeabilized and fixed with 70% ice-cold ethanol drop-wise and incubated for 15 min on ice, gently vortexing to prevent clumping. Cells were washed twice with PBS. Then, cells were resuspended in PI Staining Solution (3.8mM sodium citrate, 50 μg/ml PI (Biotium, USA), 40 μg/ml RNase A (Zymo Research, USA)) and incubated for 40 min at 37 °C in the dark. Cells were centrifuged and the supernatant was gently aspirated. Finally, the cells were resuspended in 500 μl ice cold PBS and examined on the S3e Cell Sorter (Bio-Rad Laboratories). The data of cell cycle profiles was analyzed using FlowJo software (BD Biosciences).

Illumina RNA sequencing

RNA from GRAS1 knockdown in A549 cells was isolated with RNeasy Mini kit and purified using RNA Clean & Concentrator kit. Sequencing was performed for three biological replicates each for both the knockdown and the control samples. Illumina RNA-seq libraries were prepared at the Institution for Genomic Medicine (IGM) using Illumina stranded mRNA prep after poly-A selection. Quality of the libraries was examined by Agilent BioAnalyzer, and sequencing was performed on a NovaSeq S4 with the run type of PE100. Raw paired-end FASTQ sequencing reads were mapped with STAR version 2.7.9a (Dobin et al. 2013) to human reference genome assembly GRCh38 (Schneider et al. 2017) and GENECODE gene annotation file Ensembl 104 (Frankish et al. 2018). FeatureCounts version 2.0.3 (Liao et al. 2014) was used to generate read count matrices, and DESeq2 version 1.34.0 (Love et al. 2014) analysis identified differential expression of RNA transcripts between the triplicate samples of control GapmeR or GRAS1

knockdown GapmeR treated cells. Gene ontology enrichment analysis was performed with enrichGO version 4.2.2 (Yu et al. 2012).

RNA antisense purification with mass spectrometry (RAP-MS)

RAP-MS experiments were performed from A549 cells grown in culture. The method was performed as previously described (Trang et al. 2023) with the following modifications. Cells were collected and crosslinked with 254 nm wavelength light using an XL-1500 Spectrolinker (Spectro-UV, USA). Per 20 M cells, the cell pellet was resuspended in 900 µl cold lysis buffer (10 mM Tris-HCl pH7.5, 500 mM LiCl, 0.5% n-dodecyl-β-D-maltoside, 0.2% sodium dodecyl sulfate, 0.1% sodium deoxycholate) with 1X protease inhibitor cocktail and 920 U of murine RNase inhibitor (M0314L, New England Biolabs, UK). Resuspended cell pellets were further lysed on ice by passing through an 18G blunt needle 10 times, followed by two sets of 1.5 min sonication with a Branson sonicator using the microtip (setting: 35 duty, 3.0 power output). Cell lysate was incubated with 20 U of TurboDNase (Invitrogen, USA) for 15 min at 37 ˚C to remove DNA in the lysate, and then quenched by adding 10 mM EDTA, 5 mM EGTA, and 2.5 mM TCEP. The 6 M urea hybridization buffer was added to cell lysate to a final concentration of 4 M urea, to denature non-specifically interacting proteins. Afterwards, the lysis of 20 M cells was pre-cleared by incubation with 125 µl of MyOne C1 Streptavidin beads (Invitrogen, USA) at 45 ˚C for 30 min. Biotinylated 90-mer DNA probes for RNA capture (10 µg of probes for GRAS1, 5 µg of probes each for U1 and Luciferase) were mixed with pre-cleared lysate and incubated at 45 ˚C for 2 hours with mixing at 1000 rpm (15 s shaking, 15 s off). Complexes of biotinylated DNA probes and RNA targets were then captured on MyOne C1 Streptavidin beads by incubating at 45 ˚C for 1 hour with the same mixing setting as above. Beads were washed 4 times with 4 M urea hybridization buffer, and finally resuspended with 0.5 µl of Benzonase

(E1014, SIGMA-ALDRICH) in 500 μl Benzonase Elution Buffer (20 mM Tris pH 8.0, 2 mM MgCl2, 0.05% NLS, 0.5 mM TCEP) to eluate captured proteins. Proteins were precipitated by adding 80% TCA to final concentration to 20% for overnight incubation at 4 ˚C. Precipitated proteins were collected by centrifugation for 15 min at 10,000 x *g* and 4 ˚C. The protein pellet was resuspended with 50 μl of water containing 5% Rapigest (186002123, Waters) and incubated at 100 ˚C for 10 min. Next, 0.5 μg of trypsin was added with 37 ˚C overnight incubation and 600 rpm shaking for protein digestion. Protein samples were purified using HiPPR detergent removal resin (PI88305, VWR International) and dried completely by Speedvac (Savant) before LC-MS/MS analysis at Sanford Burnham Prebys Proteomics Core on a Thermo QExactive instrument.

Annexin V apoptosis assay

Following treatment or transfection, A549 cells were collected by trypsinization and washed in cold PBS. Then cells were resuspended in 100 μl of 1X Annexin-binding buffer (10 mM Hepes adjusted to pH 7.4, 140 mM NaCl and 2.5 mM CaCl2) with 5 μl of FITC-conjugated Annexin V (A13199, Life Technologies) and 2 μl of 1 mg/ml Propidium Iodide (40017, Biotium). The cell solution was incubated for 30 minu at room temperature in the dark. After the incubation, 400 μl of 1X Annexin-binding buffer was added to the cell solution and analyzed by the S3e Cell Sorter. The raw data were analyzed by FlowJo software.

Ferroptosis analysis

Following treatment or transfection, 1 μl of 3 mM BODIPY-C11 581/591 (D3861, Life Technologies) was added to cells in each well of a 6-well plate, and incubated for 3 hrs. After the incubation, cell media with BODIPY added was transferred to a 15 ml tube, and cells were

washed with 1 ml HBSS buffer (140 mM NaCl, 5 mM KCl, 1 mM $CaCl_2$, 0.4 mM MgSO4, 0.5 mM $MgCl_2$, 0.3 mM Na_2HPO_4, 0.4 mM KH_2PO_4, 6 mM D-Glucose, and 4 mM $NaHCO_3$). The buffer and cells harvested by trypsin were collected in the corresponding 15 ml tube and centrifuged at 300 x *g* for 3 min. The supernatant was removed, and the pellet was resuspended with 500 µl HBSS for FACS analysis using the S3e Cell Sorter. The raw data were analyzed by FlowJo software.

MATERIAL AVAILABILITY

All unique/stable reagents generated in this study are available from the Lead Contact with a completed Materials Transfer Agreement and/or a payment if there is potential for commercial application. Further information and requests for resources and reagents should be directed to the lead contact, Colleen A. McHugh (c1mchugh@ucsd.edu).

AUTHOR CONTRIBUTIONS

Conceptualization, T.S., C.A.M.; methodology, T.S., L.K., C.A.M.; validation, T.S., L.K., D.C. J.Z; formal analysis, T.S., L.K., D.C., J.Z., V.C.; investigation, T.S., L.K., D.C., J.Z., N.C., C.H., C.A.M.; supervision, C.A.M; writing and revision of draft T.S., L.K., D.C., J.Z., N.C., V.C., C.H., C.A.M.; funding acquisition, C.A.M.

DECLARATION OF INTERESTS

The authors declare no competing interests.

ACKNOWLEDGEMENTS

This work was supported by the Chemistry and Biochemistry Department of the University of California San Diego, an NIH/NIGMS R00 GM120494 award to C.A.M., a Ruth L. Kirschstein National Research Service Award NIH/NCI T32 CA009523 to T.S., the University of California Cancer Research Coordinating Committee grant support C21CR2119 to C.A.M. with Diversity Supplement to C.H., an American Chemical Society Bridge Program (ACS-BP) grant to N.C., and the Dean of Physical Sciences Undergraduate Summer Research Awards to L.K. and C.H.

This publication includes data generated on the NovaSeq 6000 at the UC San Diego Institute for Genomic Medicine and supported by the Moores Cancer Center grant P30CA023100.

REFERENCES

Bin, J., Nie, S., Tang, Z., Kang, A., Fu, Z., Hu, Y., ... & Jiang, J. (2021). Long noncoding RNA EPB41L4A-AS1 functions as an oncogene by regulating the Rho/ROCK pathway in colorectal cancer. *Journal of Cellular Physiology*, 236(1), 523-535.

Burgute BD, Peche VS, Steckelberg AL, Glöckner G, Gaßen B, Gehring NH, Noegel AA. NKAP is a novel RS-related protein that interacts with RNA and RNA binding proteins. *Nucleic Acids Research*. 2014 Mar;42(5):3177-93. doi: 10.1093/nar/gkt1311. Epub 2013 Dec 17. PMID: 24353314; PMCID: PMC3950704.

Chen D, Li Z, Yang Q, Zhang J, Zhai Z, Shu HB. Identification of a nuclear protein that promotes NF-κB activation. *Biochemical and Biophysical Research Communications*. 2003 Oct 24;310(3):720-4. doi: 10.1016/j.bbrc.2003.09.074. PMID: 14550261.

Chen, X., Kang, R., Kroemer, G. et al. Broadening horizons: the role of ferroptosis in cancer. *Nature Reviews Clinical Oncology* 18, 280–296 (2021).

Cui, P., Zhao, X., Liu, J., Chen, X., Gao, Y., Tao, K., ... & Zhang, X. (2020). miR-146a interacting with lncRNA EPB41L4A-AS1 and lncRNA SNHG7 inhibits proliferation of bone marrow-derived mesenchymal stem cells. *Journal of Cellular Physiology*, 235(4), 3292-3308.

Delshad, E., Shamsabadi, F. T., Bahramian, S., Mehravar, F., Maghsoudi, H., & Shafiee, M. (2019). In silico identification of novel lncRNAs with a potential role in diagnosis of gastric cancer. *Journal of Biomolecular Structure and Dynamics. 38*(7), 1954–1962. https://doi.org/10.1080/07391102.2019.1624615

Dixon, S. J., & Stockwell, B. R. (2019). The hallmarks of ferroptosis. *Annual Review of Cancer Biology*, 3(1), 35–54.

Dobin, A., Davis, C. A., Schlesinger, F., Drenkow, J., Zaleski, C., Jha, S., Batut, P., Chaisson, M., & Gingeras, T. R. (2013). STAR: ultrafast universal RNA-seq aligner. *Bioinformatics (Oxford, England)*, *29*(1), 15–21. https://doi.org/10.1093/bioinformatics/bts635

Frankish, A., Diekhans, M., Ferreira, A. M., Johnson, R., Jungreis, I., Loveland, J., Mudge, J. M., Sisu, C., Wright, J., Armstrong, J., Barnes, I., Berry, A., Bignell, A., Carbonell Sala, S., Chrast, J., Cunningham, F., Di Domenico, T., Donaldson, S., Fiddes, I. T., García Girón, C., … Flicek, P. (2019). GENCODE reference annotation for the human and mouse genomes. *Nucleic Acids Research*, *47*(D1), D766–D773. https://doi.org/10.1093/nar/gky955

Gagnon, S. J., Ennis, F. A., & Rothman, A. L. (1999). Bystander target cell lysis and cytokine production by dengue virus-specific human CD4+ cytotoxic T-lymphocyte clones. *Journal of Virology*, *73*(5), 3623-3629.

Kastan, M. B., Canman, C. E., & Leonard, C. J. (1995). P53, cell cycle control and apoptosis: implications for cancer. *Cancer and Metastasis Reviews*, 14, 3-15.

Kazemzadeh, M., Safaralizadeh, R., & Orang, A. V. (2015). LncRNAs: emerging players in gene regulation and disease pathogenesis. *Journal of Genetics*, *94*, 771-784.

Lakin, N., Jackson, S. Regulation of p53 in response to DNA damage. *Oncogene* 18, 7644–7655 (1999).

Li, J., Cao, F., Yin, Hl. et al. Ferroptosis: past, present and future. *Cell Death Dis* 11, 88 (2020).

Li, T., Chen, L., Cheng, J. et al. SUMOylated NKAP is essential for chromosome alignment by anchoring CENP-E to kinetochores. *Nature Communications* 7, 12969 (2016).

Liao Y., Smyth G.K. and Shi W. (2014). featureCounts: an efficient general purpose program for assigning sequence reads to genomic features. *Bioinformatics*, 30(7):923-30.

Liu SJ, Horlbeck MA, Cho SW, Birk HS, Malatesta M, He D, et al. CRISPRi-based genome-scale identification of functional long noncoding RNA loci in human cells. *Science*. 2017 Jan 6;355(6320):eaah7111.

Liu, J., Chen, S. J., Hsu, S. W., Zhang, J., Li, J. M., Yang, D. C., Gu, S., Pinkerton, K. E., & Chen, C. H. (2021). MARCKS cooperates with NKAP to activate NF-κB signaling in smoke-related lung cancer. *Theranostics*, 11(9), 4122–4136.

Love M.I., Huber W., Anders S. (2014). "Moderated estimation of fold change and dispersion for RNA-seq data with DESeq2." *Genome Biology*, **15**, 550. doi:10.1186/s13059-014-0550-8.

Ma Q, Hou L, Gao X, Yan K. NKAP promotes renal cell carcinoma growth via AKT/mTOR signalling pathway. *Cell Biochemistry and Function.* 2020 Jul;38(5):574-581. doi: 10.1002/cbf.3508. Epub 2020 Feb 7. PMID: 32032976.

Mah, L. J., El-Osta, A., & Karagiannis, T. C. (2010). γH2AX: a sensitive molecular marker of DNA damage and repair. *Leukemia*, 24(4), 679-686.

Martinez, A. M., Kim, A., & Yang, W. S. (2020). Detection of Ferroptosis by BODIPY™ 581/591 C11. *Methods in Molecular Biology* (Clifton, N.J.), 2108, 125–130.

McHugh, C. A., Russell, P., & Guttman, M. (2014). Methods for comprehensive experimental identification of RNA-protein interactions. *Genome Biology*, *15*(1), 203. https://doi.org/10.1186/gb4152

McHugh, C.A., Chen, C.K., Chow, A., Surka, C.F., Tran, C., McDonel, P., Pandya-Jones, A., Blanco, M., Burghard, C., Moradian, A. and Sweredoski, M.J., 2015. The Xist lncRNA interacts directly with SHARP to silence transcription through HDAC3. *Nature*, *521*(7551), pp.232-236.

Okuda, Hidenobu, et al. "A novel transcriptional factor Nkapl is a germ cell-specific suppressor of Notch signaling and is indispensable for spermatogenesis." *PLoS One* 10.4 (2015): e0124293.

Pajerowski, A. G., Nguyen, C., Aghajanian, H., Shapiro, M. J., & Shapiro, V. S. (2009). NKAP is a transcriptional repressor of notch signaling and is required for T cell development. *Immunity*, 30(5), 696-707.

Roberts, T. C., Morris, K. V., & Weinberg, M. S. (2014). Perspectives on the mechanism of transcriptional regulation by long non-coding RNAs. *Epigenetics,* 9(1), 13-20.

Schneider, V. A., Graves-Lindsay, T., Howe, K., Bouk, N., Chen, H. C., Kitts, P. A., Murphy, T. D., Pruitt, K. D., Thibaud-Nissen, F., Albracht, D., Fulton, R. S., Kremitzki, M., Magrini, V., Markovic, C., McGrath, S., Steinberg, K. M., Auger, K., Chow, W., Collins, J., Harden, G., … Church, D. M. (2017). Evaluation of GRCh38 and de novo haploid genome assemblies demonstrates the enduring quality of the reference assembly. *Genome Research*, *27*(5), 849–864. https://doi.org/10.1101/gr.213611.116

Shapiro, M. J., Anderson, J., Lehrke, M. J., Chen, M., Nelson Holte, M., & Shapiro, V. S. (2019). NKAP regulates senescence and cell death pathways in hematopoietic progenitors. *Frontiers in Cell and Developmental Biology*, 7, 214.

Shu W, Liu G, Dai Y, Feng A, Chen Z, Han J, Li X. The oncogenic role of NKAP in the growth and invasion of colon cancer cells. *Oncology Reports*. 2019 Nov;42(5):2130-2138. doi: 10.3892/or.2019.7322. Epub 2019 Sep 18. PMID: 31545474.

Shu, C. H., Yang, W. K., Shih, Y. L., Kuo, M. L., & Huang, T. S. (1997). Cell cycle G2/M arrest and activation of cyclin-dependent kinases associated with low-dose paclitaxel-induced sub-G1 apoptosis. *Apoptosis*, *2*, 463-470.

Sun S, Gao T, Pang B, Su X, Guo C, Zhang R, Pang Q. RNA binding protein NKAP protects glioblastoma cells from ferroptosis by promoting SLC7A11 mRNA splicing in an m6A-dependent manner. *Cell Death & Disease.* 2022 Jan 21;13(1):73. doi: 10.1038/s41419-022-04524-2. PMID: 35064112; PMCID: PMC8783023.

Toné, S., Sugimoto, K., Tanda, K., Suda, T., Uehira, K., Kanouchi, H., Samejima, K., Minatogawa, Y., & Earnshaw, W. C. (2007). Three distinct stages of apoptotic nuclear

condensation revealed by time-lapse imaging, biochemical and electron microscopy analysis of cell-free apoptosis. *Experimental Cell Research*, *313*(16), 3635–3644.

Trang, N., Su, T., Hall, S., Boutros, N., Kong, B., Huang, C., & McHugh, C. A. (2023). Streamlined Purification of RNA-Protein Complexes Using UV Cross-Linking and RNA Antisense Purification. *Methods in Molecular Biology (Clifton, N.J.)*, *2666*, 213–229. https://doi.org/10.1007/978-1-0716-3191-1_16

Uramoto, H., & Tanaka, F. (2014). Recurrence after surgery in patients with NSCLC. *Translational Lung Cancer Research*, *3*(4), 242.

Wang, M., Zheng, S., Li, X., Ding, Y., Zhang, M., Lin, L., Xu, H., Cheng, Y., Zhang, X., Xu, H. and Li, S., 2020. Integrated analysis of lncRNA-miRNA-mRNA ceRNA network identified lncRNA EPB41L4A-AS1 as a potential biomarker in non-small cell lung cancer. *Frontiers in Genetics*, *11*, p.511676.

Wei Y, Wang Y, Zang A, Wang Z, Fang G, Hong D. MiR-4766-5p inhibits the development and progression of gastric cancer by targeting NKAP. *OncoTargets and Therapy*. 2019 Oct 16;12:8525-8536. doi: 10.2147/OTT.S220234. PMID: 31802890; PMCID: PMC6801498.

Xu, T, Ding, W, Ji, X, et al. Molecular mechanisms of ferroptosis and its role in cancer therapy. *Journal of Cellular and Molecular Medicine.* 2019; 23: 4900– 4912.

Yang, F., & Lv, S. (2022). LncRNA EPB41L4A-AS1 Regulates Cell Proliferation, Apoptosis and Metastasis in Breast Cancer. *Annals of Clinical & Laboratory Science*, *52*(1), 3-11.

Yu G., Wang L.G., Han Y., He Q.Y. clusterProfiler: an R package for comparing biological themes among gene clusters. *OMICS: A Journal of Integrative Biology* 2012, 16(5):284-287. doi:[10.1089/omi.2011.0118](http://dx.doi.org/10.1089/omi.2011.0118)

Zhu, Y., Liu, Q., Liao, M., Diao, L., Wu, T., Liao, W., ... & Zhang, Y. (2019). Overexpression of lncRNA EPB41L4A-AS1 induces metabolic reprogramming in trophoblast cells and placenta tissue of miscarriage. *Molecular Therapy-Nucleic Acids*, 18, 518-532.

Figure 1: GRAS1 non-coding RNA knockdown and overexpression affect A549 cell growth.

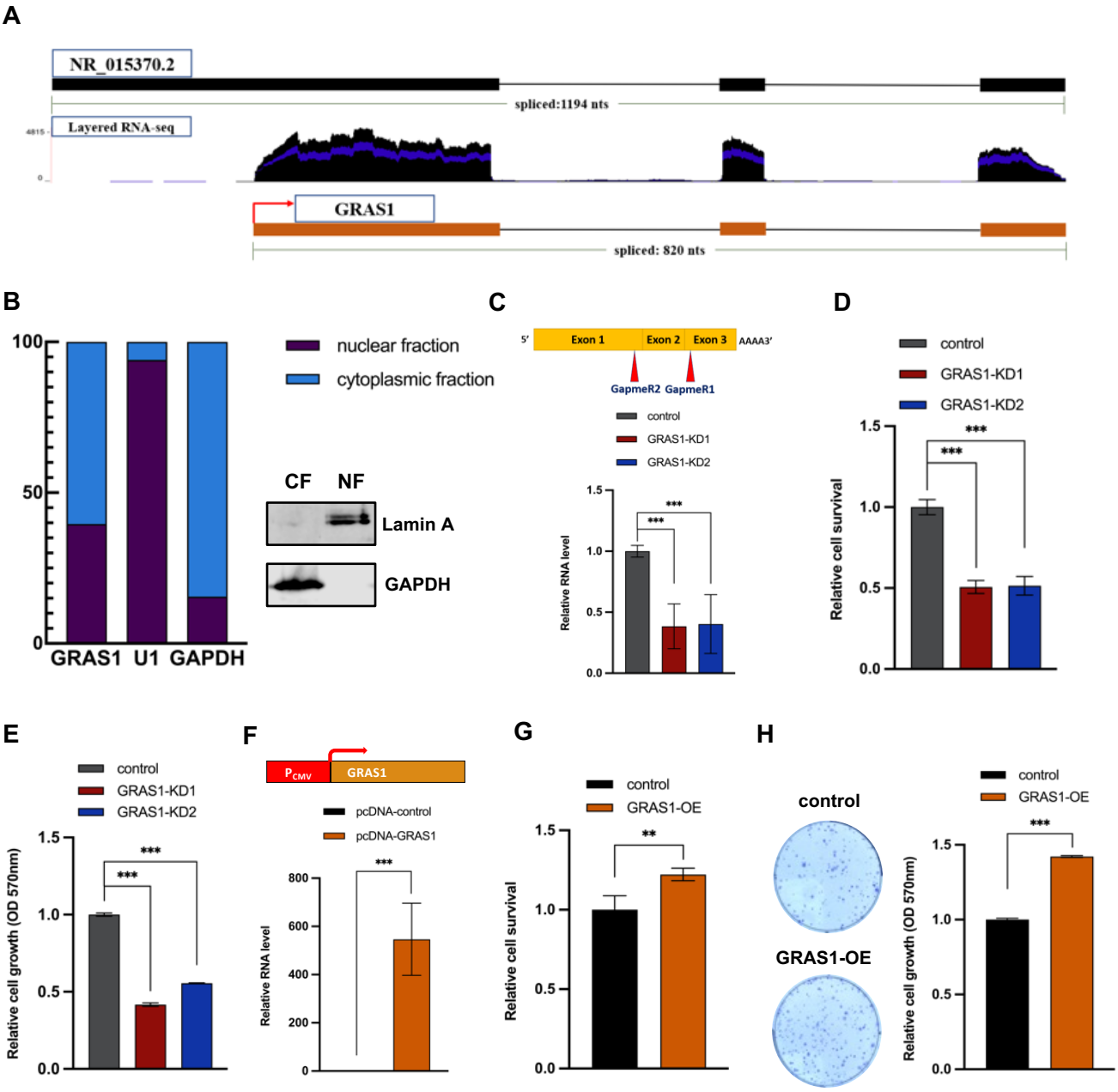

Figure 1: GRAS1 non-coding RNA knockdown and overexpression affect A549 cell growth.

(A) GRAS1 long non-coding RNA locus and ENCODE RNA-seq expression data from the UCSC Genome Browser.

(B) Analysis of GRAS1 RNA localization in cytoplasmic and nuclear fractions of A549 cells. U1 snRNA was used as a nuclear marker and GAPDH mRNA was used as a cytoplasmic marker. Lamin A and GAPDH immunoblots of the purified cytoplasmic fraction (CF) and nuclear fraction (NF) were used to monitor cell fractionation.

(C) Analysis of GRAS1 knockdown efficiency in A549 cells transfected with control GapmeR compared with GRAS1 GapmeR1 or GapmeR2, normalized to GAPDH control mRNA.

(D) MTT assay for survival of A549 cells treated with control GapmeR compared with GRAS1 GapmeR1 or GRAS1 GapmeR2.

(E) Colony formation assay of A549 cells treated with control GapmeR compared with GRAS1 GapmeR1 or GRAS1 GapmeR2. The average absorbance of solubilized crystal violet stain in each sample was measured in three independent experiments.

(F) Analysis of GRAS1 RNA expression in A549 cells treated with control pcDNA vector compared with pcDNA-GRAS1 overexpression vector by RT-qPCR, normalized to GAPDH control mRNA.

(G) MTT assay for survival of A549 cells transfected with control pcDNA vector compared with pcDNA-GRAS1 overexpression vector.

(H) Colony formation assay of A549 cells transfected with control pcDNA vector compared with pcDNA-GRAS1 overexpression vector. Representative image of control and GRAS1 overexpression colonies (left panel). Quantification of solubilized crystal violet stain from each plate was measured in three independent experiments (right panel).

Error bars represent SD. (ns) $P>0.05$; (*) $P \leq 0.05$; (**) $P \leq 0.01$; (***) $P < 0.001$ by two-tailed Student's t-test.

Figure 2: GRAS1 knockdown cells increase transcription of DNA damage response and cell cycle rela

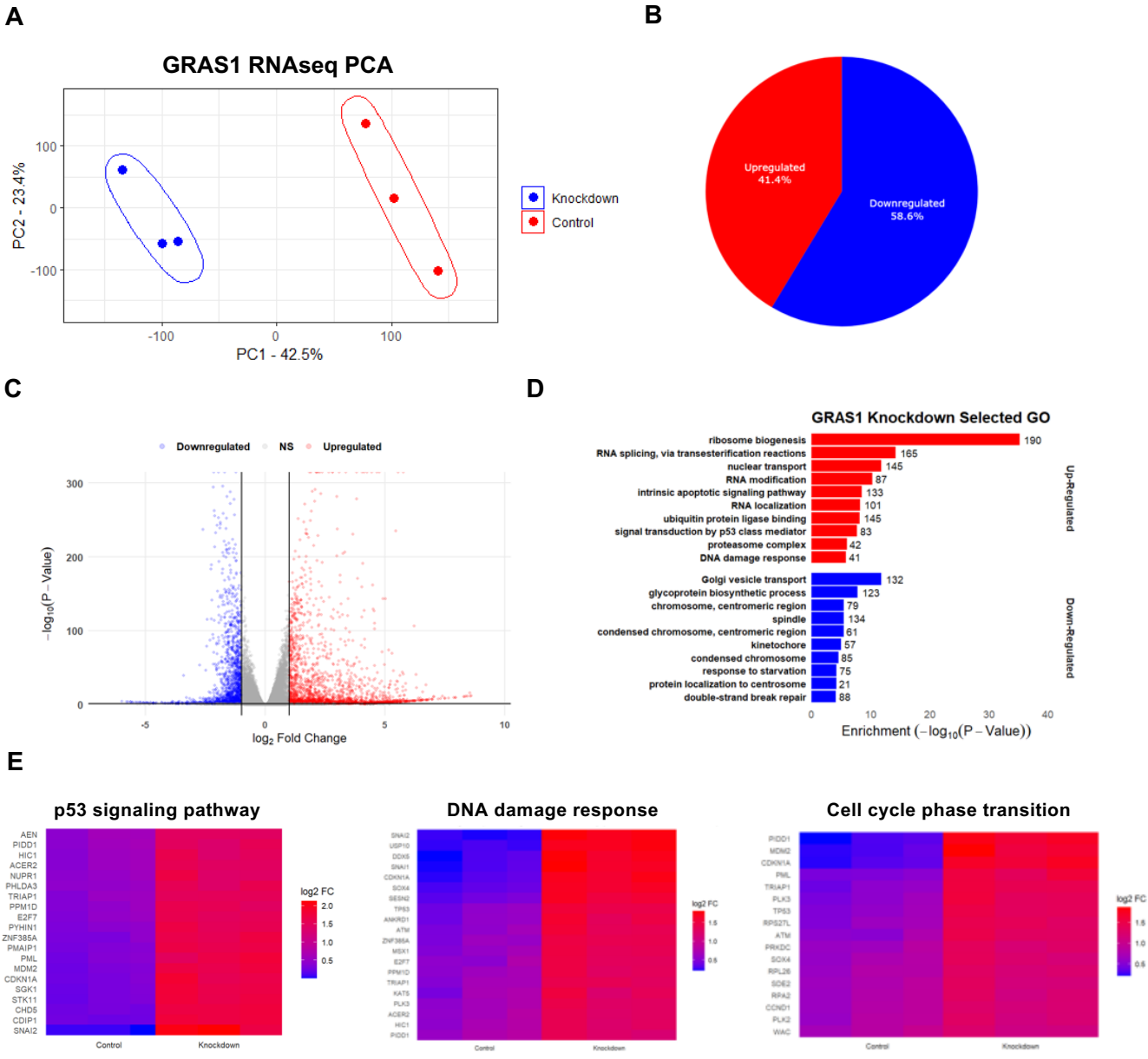

Figure 2: GRAS1 knockdown cells increase transcription of DNA damage response and cell cycle related genes.

(A) Principal component analysis (PCA) of normalized RNA-seq transcripts per million (TPM) from RNA sequencing of A549 cells transfected with control GapmeR (red) compared with GRAS1 GapmeR1 (blue). Three biological replicates were performed for each sample.

(B) Percentage of upregulated (red) and downregulated (blue) differentially expressed genes in GRAS1 knockdown cells compared to control cells.

(C) Volcano plot of differentially expressed genes in control GapmeR compared to GRAS1 GapmeR1 knockdown samples in A549 RNA-seq data. Red and blue points mark the genes with significantly increased or decreased expression, respectively.

(D) Gene Ontology enrichment analysis of selected biological processes in up- and down-regulated genes between control GapmeR and GRAS1 GapmeR1 transfected A549 cells.

(E) Relative expression of the top twenty dysregulated genes from the p53 signaling pathway, the DNA damage response, and mitotic G1/S transition after GRAS1 knockdown.

Error bars represent SD. (ns) $P>0.05$; (***) $P < 0.001$ by two-tailed Student's t-test.

Figure 3: GRAS1 knockdown causes accumulation of multiple DNA damage foci and cell death

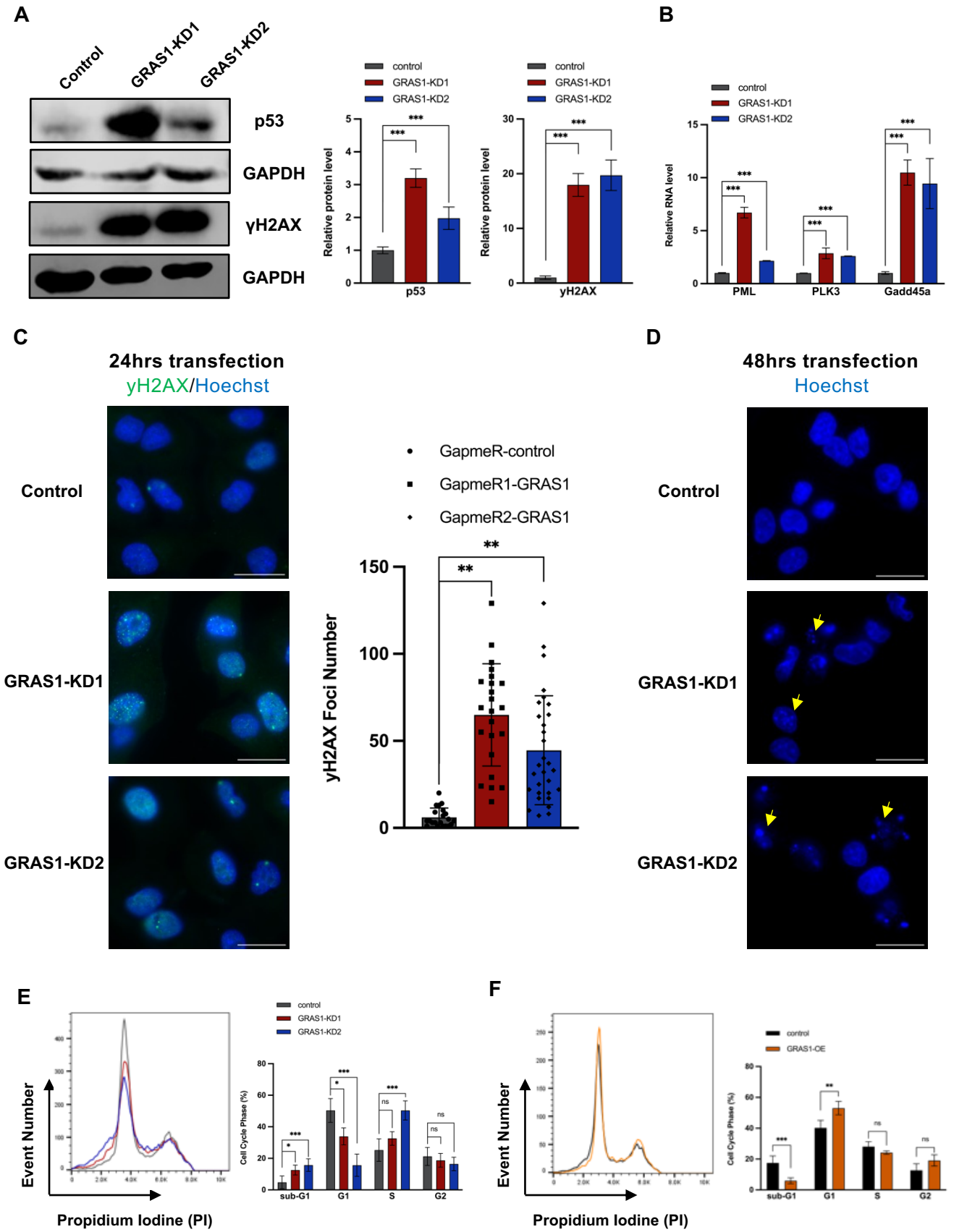

Figure 3: GRAS1 knockdown causes accumulation of multiple DNA damage foci and cell death.

(A) Western blot of p53 and γH2AX in cells treated with control GapmeR, GRAS1 GapmeR1 or GRAS1 GapmeR2 (left panel). Quantification of p53 and γH2AX expression was calculated after normalization to the GAPDH loading control for each sample (right panel).

(B) Expression of PML, PLK3, and Gadd45a mRNA levels in A549 cells treated with control GapmeR compared with GRAS1 GapmeR1 or GRAS1 GapmeR2 by RT-qPCR.

(C) Measurement of γH2AX foci (green) and Hoescht DNA stain (blue) after 24 hours of transfection with GRAS1 GapmeR1 or GRAS1 GapmeR2 compared to control GapmeR. Representative images (left panel) and the quantification of γH2AX foci per cell from 3 independent experiments are shown (right panel). The scale bar represents 25 μm.

(D) Representative images of Hoechst DNA stain (blue) in A549 cells treated with control GapmeR compared with GRAS1 GapmeR1 or GRAS1 GapmeR2 after 48 hours of transfection. Yellow arrows indicate regions of nuclear fragmentation. The scale bar represents 25 μm.

(E) Cell cycle analysis of GRAS1 knockdown cells. Representative images of cell cycle analysis by propidium iodide (PI) staining in flow cytometry for A549 transfected with control GapmeR, GRAS1 GapmeR1, or GRAS1 GapmeR2 (left panel). Quantification of the proportion of cells in each cell cycle phase (right panel).

(F) Cell cycle analysis of GRAS1 overexpression cells. Representative images of cell cycle analysis by PI staining in flow cytometry for A549 transfected with control vector or GRAS1 overexpression vector (left). Quantification of the proportion of cells in each cell cycle phase (right).

Error bars represent SD. (***) $P < 0.001$ by two-tailed Student's t-test.

Figure 4: GRAS1 non-coding RNA binds and stabilizes NF-κB activating protein (NKAP)

A

RAP-MS Purification

UV_{254nm} crosslinking in live cells

↓

Lysis and hybridization of antisense biotinylated probes to RNA

↓

Capture of RNA-protein complexes on streptavidin beads

↓

Wash with highly denaturing buffers

↓

Protein elution and mass spectrometry

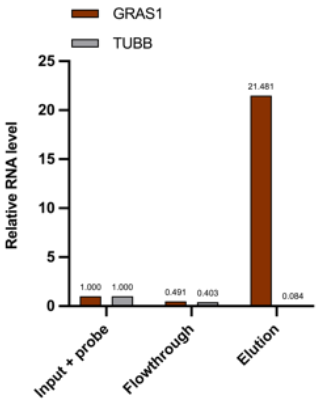

B

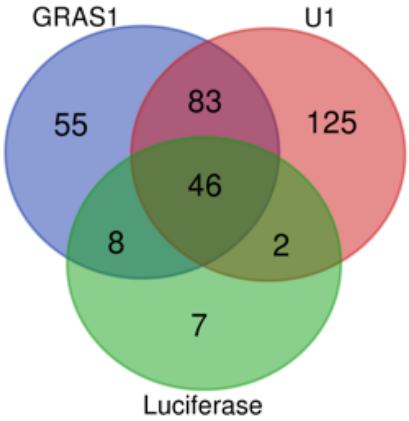

C

GRAS1 interacting proteins

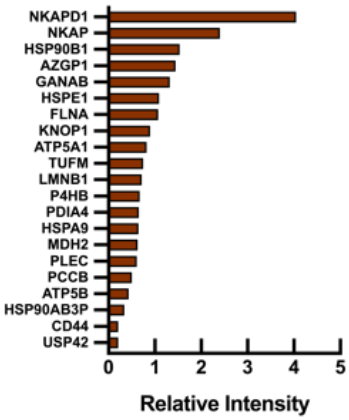

Protein name	Molecular weight (KDa)
NKAPD1	34.109
NKAP	47.138
HSP90B1	92.468
AZGP1	34.258
GANAB	106.87
HSPE1	10.932
FLNA	280.74
KNOP1	51.588
ATP5A1	59.75
TUFM	49.541

D

RNA immunoprecipitation

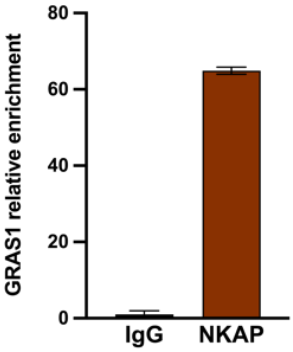

E

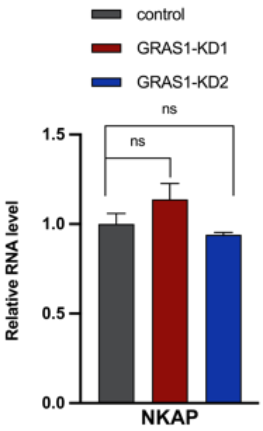

F

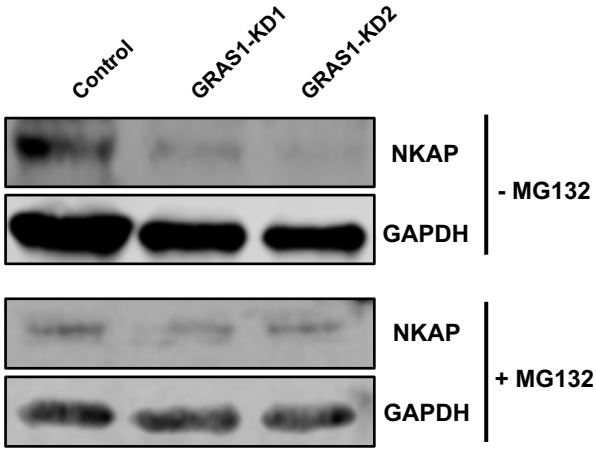

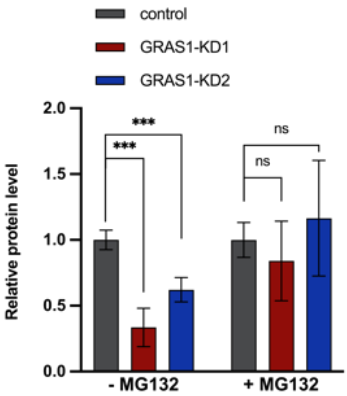

Figure 4: GRAS1 non-coding RNA binds and stabilizes NF-κB activating protein (NKAP).

(A) RNA antisense purification-qPCR experimental outline and the validation of GRAS1 RNA capture and recovery by biotinylated antisense oligonucleotide probes against GRAS1 (right panel). RT-qPCR on GRAS1 RNA and TUBB control mRNA in three fractions, including input with probes added, unbound sample flowthrough, and elution.

(B) Total proteins identified in RAP-MS of GRAS1 RNA, U1 snoRNA positive control, and luciferase mRNA negative control elution samples.

(C) GRAS1 interactome proteins identified by RAP-MS, with at least two unique peptides, after excluding proteins that were also found in U1 and luciferase control captures (left panel). The top ten GRAS1-interacting proteins and their molecular weights (right panel).

(D) GRAS1 RNA enrichment measured by RT-qPCR after immunoprecipitation of NKAP, compared to immunoprecipitation with IgG control antibody.

(E) RT-qPCR for NKAP mRNA expression in A549 cells treated with control GapmeR compared to GRAS1 GapmeR knockdown.

(F) Western blot of NKAP in control GapmeR treated cells compared to GRAS1 GapmeR1 or GRAS1 GapmeR2 knockdown under normal culture conditions (top) or with 5 μM MG132 treatment (bottom). Quantification of NKAP expression was calculated after normalizing to GAPDH loading control (right).

Error bars represent SD. (**) $P \leq 0.01$; (***) $P < 0.001$ by two-tailed Student's t-test.

Figure 5: NKAP overexpression reverses the lipid peroxidation induced by GRAS1 knockdown.

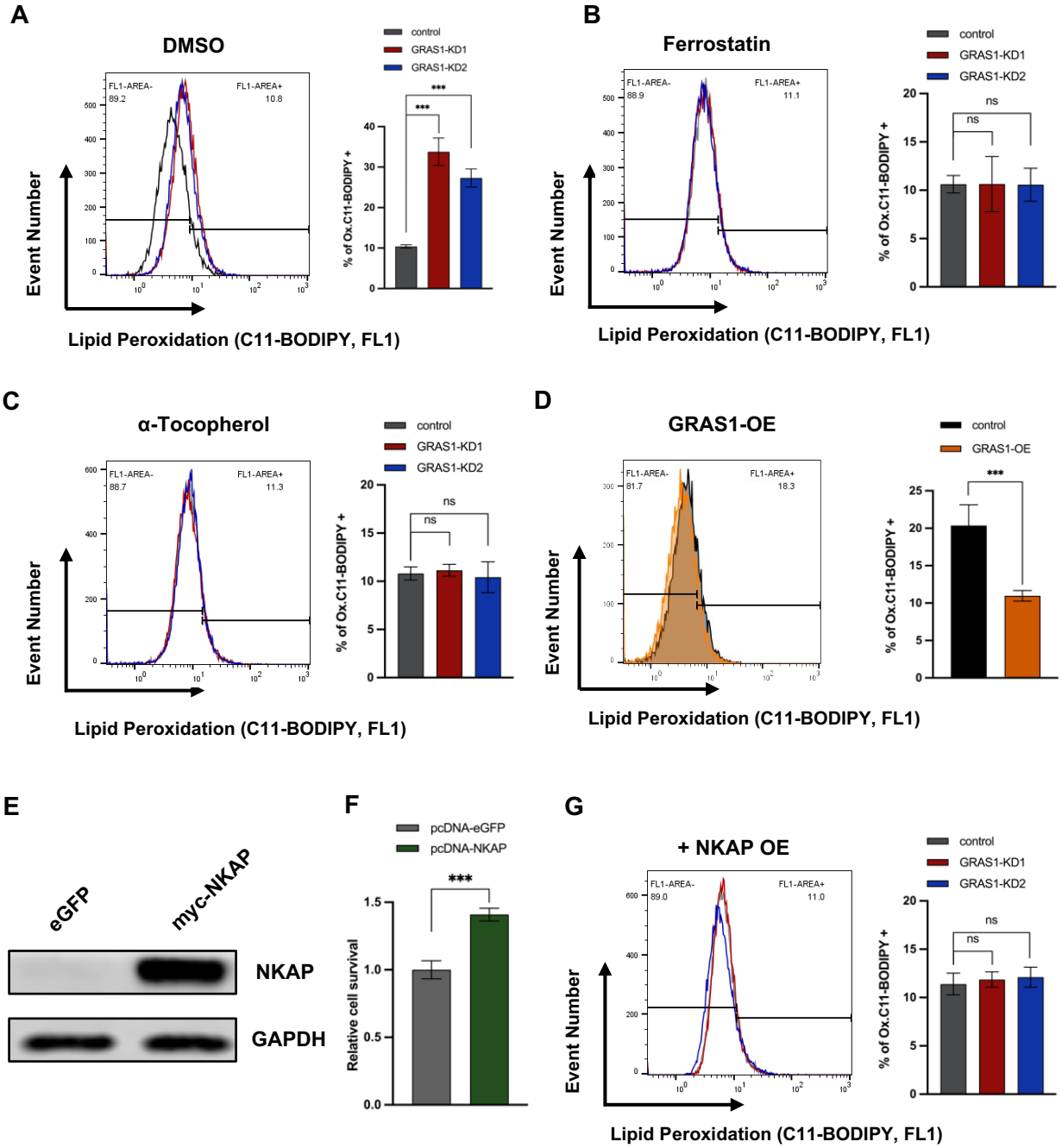

Figure 5: NKAP overexpression reverses the lipid peroxidation induced by GRAS1 knockdown.

(A) C11-BODIPY measurement of lipid peroxidation in A549 cells treated with control GapmeR compared with GRAS1 GapmeR1 or GRAS1 GapmeR2. Representative flow cytometry results (left panel) and quantification (right panel) are shown.

(B) Lipid peroxidation level of GRAS1 knockdown cells after treatment with the ferroptosis inhibitor ferrostatin.

(C) Lipid peroxidation level of GRAS1 knockdown cells after treatment with the antioxidant α-tocopherol.

(D) C11-BODIPY measurement of lipid peroxidation in A549 cells transfected with control vector compared with GRAS1 overexpression vector

(E) Western blot of NKAP levels in A549 transfected with eGFP control vector or myc-tagged NKAP overexpression vector.

(F) Cell survival measured by MTT assay in A549 cells transfected with eGFP control vector or myc-tagged NKAP vector.

(G) Lipid peroxidation level measured by C11-BODIPY staining in flow cytometry of A549 cells transfected with eGFP control vector or GRAS1 overexpression vector.

Error bars represent SD. (ns) $P>0.05$; (**) $P \leq 0.01$; (***) $P < 0.001$ by two-tailed Student's t-test.

Figure 6: Overexpression of NKAP prevents DNA damage in GRAS1 knockdown cells.

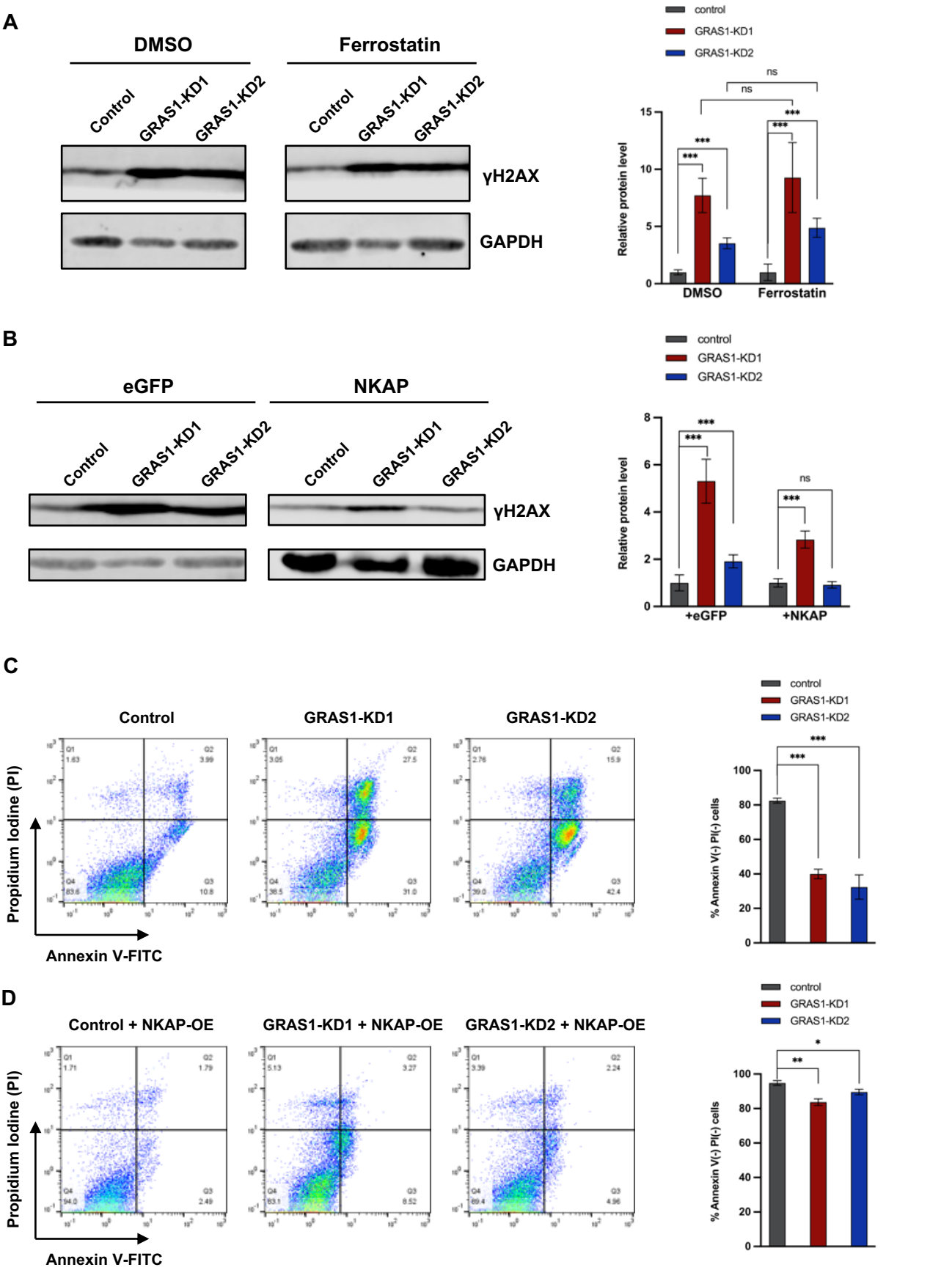

Figure 6: Overexpression of NKAP prevents DNA damage in GRAS1 knockdown cells.

(A) Western blot of γH2AX in A549 after treatment with DMSO control or ferrostatin (left panel). Quantification of expression in γH2AX was calculated after normalizing to GAPDH (right panel).

(B) Western blot of γH2AX in A549 cells co-transfected with eGFP control vector or myc-tagged NKAP vector, and treated with control GapmeR, GRAS1 GapmeR1, or GRAS1 GapmeR2.

(C) GRAS1 induced A549 cell death, as assessed by flow cytometry with Annexin V/PI staining. Representative results of A549 with control GapmeR, GRAS1 GapmeR1 or GRAS1 GapmeR2 treatment (left panel). Quantification on percentage of Annexin V-negative/ PI-negative A549 cells treated with control GapmeR compared with GRAS1 GapmeR1 or GRAS1 GapmeR2 (right panel).

(D) NKAP overexpression increases the percentage of live cells from GRAS1 knockdown, as assessed by flow cytometry with Annexin V/PI staining. Representative results (left panel), and quantification of cells are shown (right panel).

Error bars represent SD. (ns) $P>0.05$; (**) $P \leq 0.01$; (***) $P < 0.001$ by two-tailed Student's t-test.

Supplementary Figure 1

A

RNAseq sample	Read Length	Number of Reads	% Uniquely Mapped
Control	101	24414878	88.74
Control	101	30631523	88.85
Control	101	35511447	87.32
GRAS1-KD	101	42257830	89.39
GRAS1-KD	101	37652306	88.91
GRAS1-KD	101	39773180	86.26

B

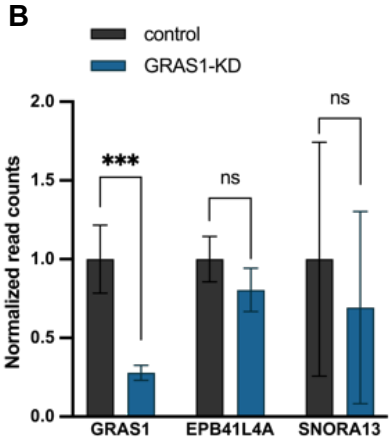

Figure S1: GRAS1 knockdown does not affect RNA expression of GRAS1 nearby genes.

(A) The statistics of sequence length, number of reads, and percentage of uniquely mapped in the RNA sequencing data.

(B) RNA expression of GRAS1, EPB41L4A, and SNORA13 in control and GRAS1 knockdown groups based on read counts in RNA sequencing.

Error bars represent SD. (ns) $P>0.05$ by two-tailed Student's t-test.

Supplementary Figure 2

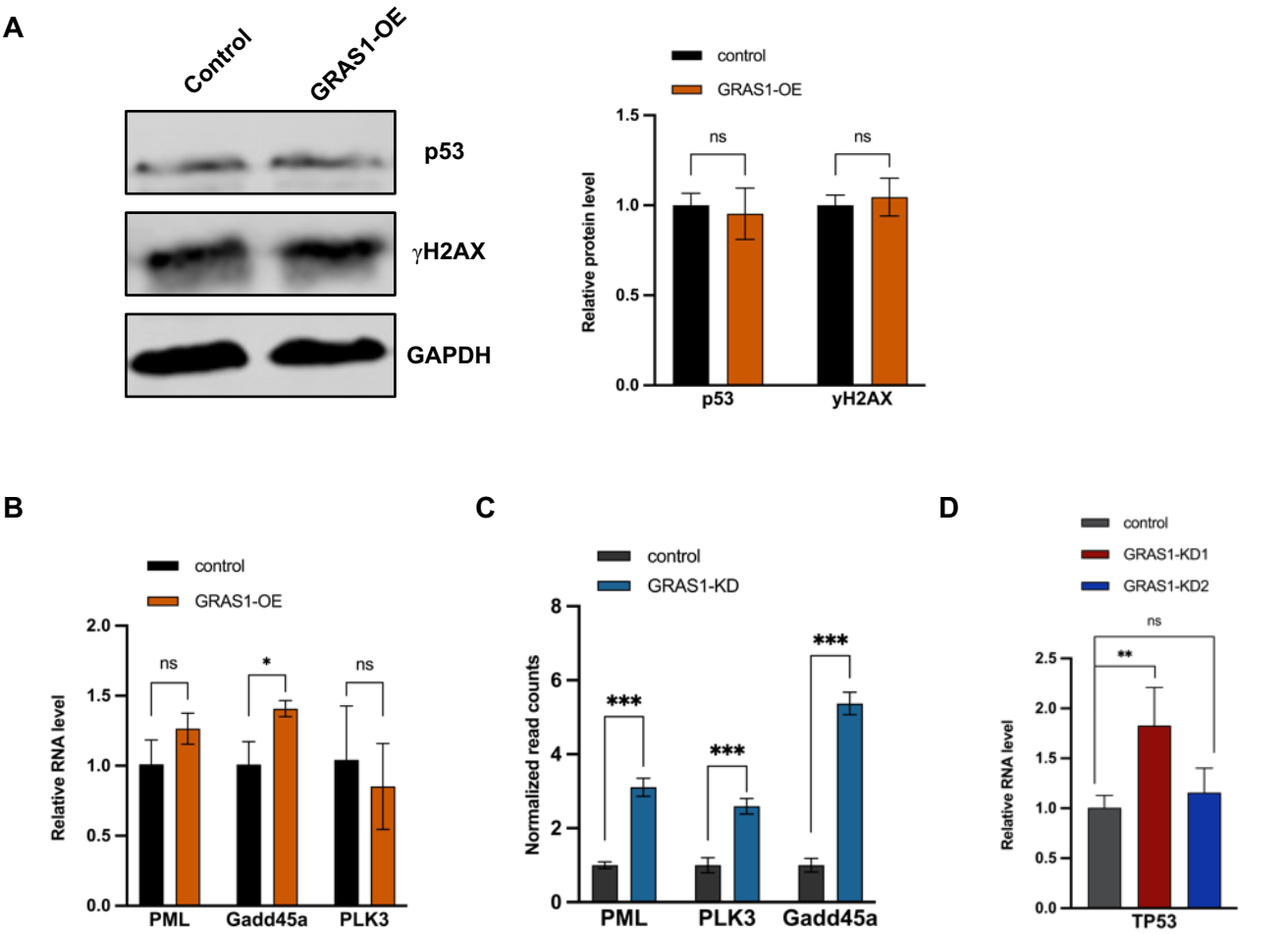

Figure S2: GRAS1 overexpression has no effect on p53 and γH2AX expression.

(A) Western blot of p53 level and γH2AX level in A549 transfected with control vector compared with GRAS1 overexpression vector (left). Quantification of p53 and γH2AX expression was performed after normalizing to GAPDH control (right).

(B) mRNA expression of PML, Gadd45a, and PLK3 in A549 cells treated with control vector compared with GRAS1 overexpression vector by RT-qPCR.

(C) RNA expression of PML, PLK3, and Gadd45a in control and GRAS1 knockdown groups based on read counts in RNA sequencing.

(D) RT-qPCR for TP53 mRNA expression in A549 cells treated with control GapmeR compared to GRAS1 GapmeR knockdown.

Error bars represent SD. (ns) $P>0.05$; (***) $P < 0.001$ by two-tailed Student's t-test.

Supplementary Figure 3

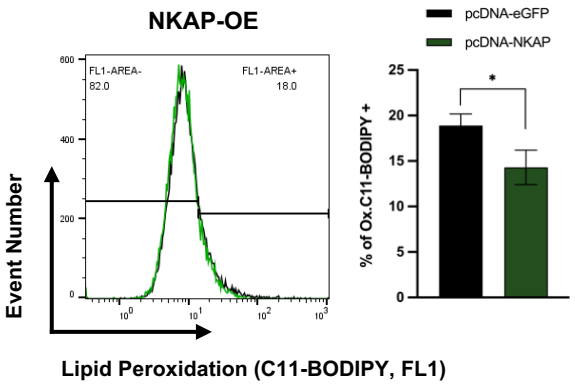

Figure S3: NKAP overexpression decreases lipid peroxidation in A549 cells.

(A) C11-BODIPY measurement of lipid peroxidation in A549 cells transfected with control vector compared with myc-tagged NKAP overexpression vector. Representative flow cytometry results (left panel) and quantification (right panel) are shown.

Error bars represent SD. (*) $P \leq 0.05$ by two-tailed Student's t-test.

Supplementary Figure 4

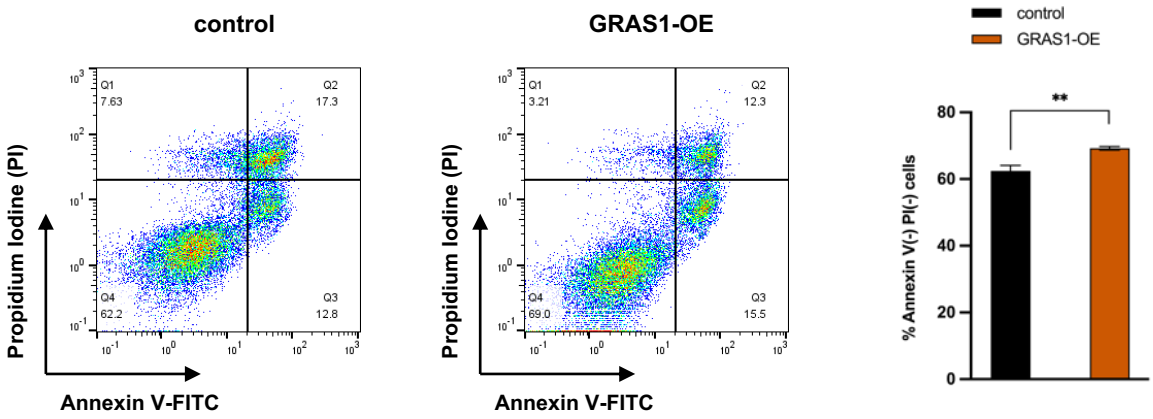

Figure S4: GRAS1 overexpression increases cell survival in A549 cells.

(A) GRAS1 protects A549 from cell death, as assessed by flow cytometry after Annexin V/PI staining. Representative images of A549 with control vector and GRAS1 overexpression vector (left). Quantification of percentage of Annexin V-negative/ PI-negative A549 cells treated with control vector compared with GRAS1 overexpression vector (right).

Error bars represent SD. (**) $P \leq 0.01$ by two-tailed Student's t-test.

REAGENTS AND SEQUENCES

Antibodies	Source	Identifier
Lamin A/C Polyclonal antibody	Proteintech	Cat No. 10298-1-AP
GAPDH Monoclonal antibody	Proteintech	Cat No. 60004-1-Ig
P53 Polyclonal antibody	Proteintech	Cat No. 10442-1-AP
NF-κB p65 Polyclonal antibody	Proteintech	Cat No. 10745-1-AP
Cytochrome c Polyclonal antibody	Proteintech	Cat No. 10993-1-AP
Ubiquitin (P4D1) Mouse mAb	Cell Signaling Technology	Cat No.#3936
Phospho-Histone H2A.X (Ser139) (20E3) Rabbit mAb	Cell Signaling Technology	Cat No.#9718
Anti-NKAP antibody	Abcam	Cat No. Ab229096

RT-qPCR primers		
Target	Forward (5'-3')	Reverse (5'-3')
hGAPDH	GGG CTC TCC AGA ACA TCA TCC	GTG CAC CAC TGA CAC GTT GG
TUBB	GAT CAG TGA TGA ACA TGG CAT CG	AAA GGA CCT GAG CGA ACA GAG
TUBB	CCA GAC AAC TTT GTA TTT GGT CAG T	CGT ACC ACA TCC AGG ACA GAA T
PML	CCG TCA TAG GAA GTG AGG GCT TC	GTT TTC GGC ATC TGA GTC TTC CG
NKAP	GCT GGA AAA CGT ATC CCA CGA AG	CTG GTT CTC TTT TCG CAG TCG C
BDKRB1	GCC TGT GAC AAT GCT CCA GAA G	TTT CTG CCA CGT TCA GTT GCC G
PLK3	CTA TGT GGC TCC AGA AGT GCT G	TCC TTC AGG TCA GCC GTC TCA A
GADD45a	TGC TCA GCA AAGCCC TGA GT	GCA GGC ACA ACA CCA CGT TA
GCLC	GGA AGT GGA TGT GGA CAC CAG A	GCT TGT AGT CAG GAT GGT TTG CG
COX2	CGG TGA AAC TCT GGC TAG ACA G	GCA AAC CGT AGA TGC TCA GGG A
BACE1	GTG AGG TTA CCA ACC AGT CCT TC	CGT GGA TGA CTG TGA GAT GGC A
ANGPT1	CAA CAG TGT CCT TCA GAA GCA GC	CCA GCT TGA TAT ACA TCT GCA CAG
NR3C1	GGA ATA GGT GCC AAG GAT CTG G	GCT TAC ATC TGG TCT CAT GCT GG
hU1	TTA CCT GGC AGG GGA GAT AC	TCC CAC ATT TGG GGA AAT C
GRAS1	CCT TTT GGT GCG AGC TTG CTG T	GTC GAC TCA CCA GAC TCA GGG TG

Experimental model: Cell line		
Human cell line	Source	Identifier
A549	ATCC	No. CCL-185
K562	ATCC	No. CRL-3344
MCF7	ATCC	No. HTB-22
HEK293	ATCC	No. CRL-1573